Stoch Environ Res Risk Assess (2017) 31:1633–1648
DOI 10.1007/s00477-016-1294-7

ORIGINAL PAPER

Spatial pattern analysis using hybrid models: an application to the Hellenic seismicity

Marianna Siino[1] · Giada Adelfio[1] · Jorge Mateu[2] · Marcello Chiodi[1] · Antonino D'Alessandro[3]

Published online: 4 August 2016

Abstract Earthquakes are one of the most destructive natural disasters and the spatial distribution of their epicentres generally shows diverse interaction structures at different spatial scales. In this paper, we use a multi-scale point pattern model to describe the main seismicity in the Hellenic area over the last 10 years. We analyze the interaction between events and the relationship with geological information of the study area, using hybrid models as proposed by Baddeley et al. (2013). In our analysis, we find two competing suitable hybrid models, one with a full parametric structure and the other one based on nonparametric kernel estimators for the spatial inhomogeneity.

Keywords Hellenic earthquakes · Hybrids of Gibbs point processes · Point process residuals · Spatial covariates · Spatial point processes

✉ Marianna Siino
marianna.siino01@unipa.it

Giada Adelfio
giada.adelfio@unipa.it

Jorge Mateu
mateu@mat.uji.es

Marcello Chiodi
marcello.chiodi@unipa.it

Antonino D'Alessandro
antonino.dalessandro@ingv.it

[1] Università degli Studi di Palermo, Palermo, Italy

[2] Universitat Jaume I, Castellón, Spain

[3] Istituto Nazionale di Geofisica e Vulcanologia, National Earthquake Center, Rome, Italy

1 Introduction

Point processes are widely used to model data in the form of events in a region of the plane showing a particular spatial structure. There are applications of point process models in forestry and plant ecology, epidemiology, zoology, human and social interaction, seismology and astronomy (Baddeley et al. 2006). Often, a first question when analyzing point pattern data is whether the given data exhibit complete spatial randomness (i.e. the points are a realization of a spatial Poisson process) as opposed to exhibiting either spatial aggregation or spatial inhibition. To answer this question in the course of a descriptive analysis, second-order summary statistics are used to describe the general interaction behavior between the points in the pattern.

The cause of aggregation may be due to the heterogeneity related to an underlying environmental process, to the clustering around the points of another point process or to the interaction structure between points. For example, an inhomogeneous Poisson process with intensity function $\lambda(\cdot)$ can show apparent clusters of events in regions of relatively high intensity, although the source of such environmental heterogeneity could itself be of stochastic nature (see the Cox model setup in Cox and Isham 1980). In fact, there is ambiguity between heterogeneity that corresponds to the spatial variation of the intensity and clustering, i.e. dependence between the points of the pattern; these two aspects are difficult to untangle in a real context Illian et al. (2008). When events are clustered together, the modeling formulation is usually based on self-exiting point processes. These models are largely used to describe earthquakes characteristics, assuming that the occurrence of an event increases the probability of occurrence of other events in time and space. In particular,

Hawkes model (Hawkes and Adamopoulos 1973) or ETAS model (Ogata 1988) are examples of self-exciting point processes. Moreover, diagnostic methods based on second-order statistics for spatial and space-time interaction are shown in Adelfio (2010), Adelfio and Chiodi (2009), Adelfio and Schoenberg (2009).

On the other hand, when an inhibitive pattern is observed, an important class of processes is represented by self-correcting processes. In these models, it is assumed that each event, that occurs in a given point in time, has an inhibiting effect to the following ones. In the seismological context, self-correcting processes are represented by the strain-release models (Vere-Jones 1978), for which the fault fracture that generates earthquakes reduces the amount of strain present at the break point along the fault. An important example of self-correcting processes is the Strauss point process model (Strauss 1975) with a negative association. It is also the simplest inhibitive Markov (or Gibbs) point process (Baddeley and Møller 1989), which describes patterns characterized by a local interaction between neighbouring points.

In the context of spatial point patterns, Gibbs point processes are generally applied in the analysis of spatial interaction and inhomogeneity depending on covariate information. For example, Anwar et al. (2012) and Ye et al. (2015) use a multitype Strauss process considering geological spatial covariates to describe the spatial pattern of the aftershocks epicentres following two strong earthquakes occurred in Kashmir (Pakistan-2005) and in the Yellowstone National Park in 1975. However, Gibbs models could not be appropriate to describe strong clustering and multi-scale variations that are characteristics of most natural processes, such as earthquakes (Illian et al. 2008; Møller and Waagepetersen 2004).

Although the models cited above represent a wide variety of solutions to describe different types of spatio and spatio-temporal patterns, seismological events need complex models that are able to account for environmental heterogeneity while detecting interactions at several spatial scales, usually in terms of clustering.

Motivated by these needs, we propose using hybrid models (Baddeley et al. 2013) to analyze earthquake data. Hybrid models are used for patterns that show interactions at different spatial scales, such as human social interaction (Baddeley et al. 2013) and spatial distribution of plants (Badreldin et al. 2015). More exactly, we describe the spatial intensity of the events with a magnitude greater or equal than 4 occurred in the Hellenic area between 2005 and 2014. We characterize in a proper way the spatial interaction between events happening at several spatial scales, and the spatial inhomogeneity of the process considering the geological information available in the study area (the presence of volcanoes, plate boundaries and faults).

The paper is organized as follows. Section 2 describes the used statistical methodology. The study area and the available data are described in Sect. 3. The results of the descriptive analysis and the estimated models are presented in Sect. 4. The last section is devoted to conclusions and final remarks.

2 Methods

In this section, we report and revise some model notation of Gibbs and Hybrids of Gibbs point process models that will be used and discussed in the paper. Moreover, we give some details about estimation procedure and diagnostic techniques.

2.1 Gibbs and Hybrids of Gibbs point process models

A spatial point pattern $\mathbf{x} = \{x_1, \ldots, x_n\}$ is an unordered set of points in the region $W \subset \mathbb{R}^d$ where $n(\mathbf{x}) = n$ is the number of points and $|W| < \infty$. The class of Gibbs processes X also called Markov point processes is determined through a probability density function $f : \chi \to [0, \infty)$, where $\chi = \{\mathbf{x} \subset W : n(\mathbf{x}) < \infty\}$ is a set of point configurations contained in W. Generally any unnormalized density $f(\mathbf{x})$ that is integrable and not identical to zero can be used to define a finite point process but $f(\cdot)$ should also satisfy other properties such as the local stability. For further details about desirable properties for an unnormalized density see Møller and Waagepetersen 2004; Baddeley et al. 2015. A finite Gibbs point process is a finite simple point process defined with a density that satisfies the hereditary condition $f(\mathbf{x}) > 0 \Rightarrow f(\mathbf{y}) > 0$ for all $\mathbf{y} \subset \mathbf{x}$. Its density function can be written in the form

$$f(\mathbf{x}) = exp\left\{ V_0 + \sum_{x \in \mathbf{x}} V_1(x) + \sum_{x,y \in \mathbf{x}} V_2(x,y) + \cdots \right\} \qquad (1)$$

where V_0 is a constant and $V_k : \chi^k \to \mathbb{R} \cup \{-\infty\}$ is a symmetric function called the potential of order k, with $k = \{1, 2, \ldots\}$ (Ripley and Kelly 1977; Møller and Waagepetersen 2004). An unnormalized density f has interaction order m if $V_k = 0$ for all $k > m$. It has an interaction range equal to r if all $V_k(\mathbf{x}) = 0$ whenever $\mathbf{x}$ contains two points $x_1, x_2 \in \mathbf{x}$ such that $||x_1 - x_2|| > r$. In this paper, we refer to specific Gibbs models and combine them under a hybrid approach. In particular, we focus on Strauss and Geyer models that account for different types of point

interaction. Apart from the Poisson point process, that has interaction order equal to 1 and null interaction range, the most common Gibbs processes are the pairwise interaction processes that have $m = 2$ and a density function of the form

$$f(\mathbf{x}) = \alpha \prod_{i=1}^{n} b(x_i) \prod_{i<j} c(x_i, x_j) \tag{2}$$

where $b : W \to [0, \infty)$, $c : W \times W \to [0, \infty)$ and $\alpha > 0$ is the normalizing constant. A simple case of (2) is the homogeneous *Strauss Process* (Strauss 1975), with $b(u) = \beta > 0$ and

$$c(u, v) = \begin{cases} \gamma & if\ ||u - v|| < r \\ 1 & otherwise \end{cases} \tag{3}$$

where r is a fixed interaction distance and $0 \leq \gamma \leq 1$ is the interaction parameter. It follows that the probability density is $f(\mathbf{x}) = \beta^{n(\mathbf{x})}\gamma^{t(\mathbf{x},r)}$, where $t(\mathbf{x}, r)$ is the number of unordered pairs of distinct points in the pattern $\mathbf{x}$ that lie closer than r units apart. As a special case, the Strauss process with $\gamma = 1$ is a Poisson process with completely random points. Pairwise interaction point processes are commonly used to describe spatial events with a regular pattern (Illian et al. 2008).

On the other hand, when points present an attractive interaction, a proper Gibbs process is the homogeneous *Geyer saturation process* (Geyer 1999). It has an unnormalized density equal to

$$f(\mathbf{x}) = \beta^{n(\mathbf{x})} \prod_{i=1}^{n(\mathbf{x})} \gamma^{min(s, t(x_i, \mathbf{x}\backslash x_i))} \tag{4}$$

where $s > 0$ is the saturation parameter and $t(\cdot)$ is the number of unordered pairs of distinct points in the pattern $\mathbf{x}$ that lie closer than r units apart. The process is clustered when $\gamma > 1$ and inhibitive when $\gamma \leq 1$.

However Gibbs processes have some drawbacks when points have a strong clustering and show spatial dependence at multiple scales (Illian et al. 2008; Møller and Waagepetersen 2004; Baddeley et al. 2013).

In Baddeley et al. (2013), the authors propose hybrid models as a general way to generate multi-scale processes combining Gibbs processes.

Given m unnormalized densities $f_1, f_2, \ldots, f_m$, the hybrid density is defined as $f(\mathbf{x}) = f_1(\mathbf{x}) \times \ldots \times f_m(\mathbf{x})$. The new unnormalized density and the component densities f_i have to respect some assumptions, for more details see Baddeley et al. 2013. For example the density of the stationary hybrid process obtained considering m Geyer components (4) (with interaction ranges $r_1, \ldots r_m$ and saturation parameters $s_1, \ldots, s_m$) is

$$f(\mathbf{x}) = \beta^{n(\mathbf{x})} \prod_{i=1}^{n(\mathbf{x})} \prod_{j=1}^{m} \gamma_j^{min(s_j, t(x_i, \mathbf{x}\backslash x_i; r_j))} \tag{5}$$

where $t(u, \mathbf{x}\backslash u; r_j) = \sum_i \{\mathbf{1}||u - x_i|| \leq r_j\}$. This density indicates that the spatial interaction between points changes with the distances r_j and the parameters that capture this information are the interaction parameters γ_j. If an inhomogeneous version of (5) is considered, the value of β is replaced by a function $\beta(x_i)$ that expresses a spatial trend and it can be a function of the coordinates of the points and covariate information defined in all the study area. Generally, we can specify that the density f is a function of a vector of regular parameters θ and a vector of irregular parameters η. This distinction is important since these parameters are estimated into two different steps, as it is shown in the next paragraph. In the case of (5), the previous two parametric vectors are $\theta = \{\log(\beta), \log(\gamma_1), \ldots, \log(\gamma_m)\} = \{\theta_1, \theta_2\}$ for regular parameters and $\eta = \{(r_1, s_1), \ldots, (r_m, s_m)\}$ for the irregular ones. Moreover, the regular vector can be subdivided into parameters for the description of the spatial trend (θ_1) and parameters for the interaction effects (θ_2).

2.2 Model estimation

Generally the density function f of the point process is governed by a parameter vector ϕ, but, for a wide class of spatial process models, the likelihood is difficult to evaluate and to maximize. The pseudolikelihood of a point process is then used as an alternative (Besag 1975, 1977; Jensen et al. 1991), and it is given by

$$PL(\phi; \mathbf{x}) = \left[\prod_{i=1}^{n(\mathbf{x})} \lambda_\phi(x_i, \mathbf{x}) \right] exp\left[-\int_W \lambda_\phi(u, \mathbf{x}) du \right]$$

where $\lambda_\phi(u; \mathbf{x}) = f_\phi(\mathbf{x} \cup \{u\})/f_\phi(\mathbf{x}\backslash u)$ is the so called Papangelou conditional intensity at location $u \in W$ given $\mathbf{x}$.

In hybrid models, $\phi = \{\theta, \eta\}$ and the conditional intensity is the product of the conditional intensities of the components of the defined density f. (Baddeley et al. 2013)

$$\lambda_\phi(u, \mathbf{x}) = \exp\{B(u) + \theta_1^T V_1(u, \eta) + \theta_2^T G(u, \mathbf{x}, \eta)\} \tag{6}$$

where $B(u)$ is an offset term, $\theta_1^T V_1(u, \eta)$ is the first-order potential and $\theta_2^T G(u, \mathbf{x}, \eta)$ is the sum of terms with $k \geq 2$ in (1). The term $G(\cdot)$ accounts for the interaction effects and in the next paragraph following a hybrid approach it will be a combination of Strauss and Geyer processes. The technique that is considered in this work for computing approximate maximum pseudolikelihood estimates is

described in Baddeley and Turner (2000). The irregular parameters are estimated through the profile pseudolikelihood, maximizing $p(\eta, \mathbf{x}) = \max_\theta \log PL(\theta, \eta)$ over η. Their computation is a crucial issue both for a numerical aspect and because they may affect the interpoint interaction or the spatial trend parameters estimation. In fact, after computing $\hat{\eta}$, the vector θ is obtained by maximizing $\log PL(\theta, \hat{\eta})$.

Different specifications can be considered for the trend part ($B(u)$ and $\theta_1^T V_1(u)$) of (6). In the following sections, we apply models on earthquake data, and we consider a parametric and a non-parametric formulation for the spatial term depending on the coordinates. Moreover we explain the trend part as a parametric function of a set of spatial covariates that are defined in all the study region.

For the non-parametric specification of the spatial trend, we use a kernel estimator. Generally, given n observed events $u_1, u_2 \ldots, u_n$ in $\mathbb{R}^d$, the kernel estimator of the unknown density $f(\cdot)$ (Silverman 1986) is

$$\hat{f}_{\mathbf{\Sigma}}(u) = \frac{\sum_{i=1}^{n} w_i K(u - u_i, \mathbf{\Sigma})}{\sum_{i=1}^{n} w_i} \tag{7}$$

where $K(\cdot, \cdot)$ is a multivariate kernel function centred at the observed points, $\mathbf{\Sigma}$ is a matrix of smoothing constants with $diag(\Sigma) = \{h_x, h_y\}$ when $d = 2$ and w_i are weights. Usually the normal multivariate density is chosen for $K(\cdot, \cdot)$. In our study, we consider some of the options proposed in the **spatstat** package (Baddeley and Turner 2005) of R (R Development Core Team 2005) to determine the bandwidth for a Gaussian kernel: cross-validated bandwidth selection, likelihood cross-validation and Scott's rule. Moreover we use the FLP (Forward Likelihood for Prediction) method proposed in Chiodi and Adelfio (2011), and developed in Adelfio and Chiodi (2015a), for the estimation of the bandwidth vector $\mathbf{h} = (\mathbf{h_x}, \mathbf{h_y})$, assuming a bivariate normal kernel for the spatial distribution of the background seismicity. The FLP approach consists of a simultaneous estimation of non-parametric and parametric components of the conditional intensity (on the history $\mathcal{H}_t$ of the point process up to time t) of a branching-type model (Daley and Vere-Jones 2007) $\lambda(t, \mathbf{s}|\mathcal{H}_\mathbf{t}) = \mu \mathbf{f}(\mathbf{s}) + \tau_{\boldsymbol{\phi}}(\mathbf{t}, \mathbf{s})$. The conditional intensity is defined as the sum of a term describing the long-term variation (background) $\mu\, f(\mathbf{s})$, and one relative to the short-term variation (offsprings) $\tau_{\boldsymbol{\phi}}(t, \mathbf{s})$. In applications, the background component $\mu f(\mathbf{s})$ is usually estimated by non-parametric techniques, such as kernel estimators. In this paper, we use the FLP method to get a proper estimate of the bandwidth vector estimated with the R package **etasFLP** (Chiodi and Adelfio 2014; Adelfio and Chiodi 2015b).

2.3 Diagnostics

After fitting a model, the next step is to assess the goodness-of-fit. In this work, the diagnostic tools on residuals described in Baddeley et al. (2005) have been used to check the general fitting and if the specification of the spatial trend, covariate effects and interpoint interactions are appropriate.

Additional diagnostic tools useful for hybrid models are proposed in Baddeley et al. (2011) and they are based on the second-order summary statistics, K and G functions. Usually the Ripley's K-function Ripley (1976, 1988), that is determined by the second-order moment properties of the process, is used to detect the presence of clustering or spatial regularity comparing its value to the theoretical one under the Poisson assumption. Also the G function, that is the nearest neighbor distance of a point pattern, is used to study clustering and inhibition between points.

In Baddeley et al. (2011) , they propose new tools for model validation in the analysis of spatial point pattern data based on residual summary statistics namely, the residual K and G functions. They show that the score test for models comparison is equivalent to the residual K and G functions, that are the difference of a summary statistic $S(x)$ and its predicted value $ES(X)$ under a null model.

For example, the residual K-function is computed as the difference between the non-parametric estimated K-function ($\hat{K}_\mathbf{x}(r)$) and its compensator ($C\hat{K}_\mathbf{x}(r)$). Following Baddeley et al. (2011), under CSR (complete spatial randomness) condition and the intensity being estimated by n / $|W|$, the pseudo-residual is approximately given by

$$\begin{aligned} &2(\hat{K}_\mathbf{x}(r) - C\hat{K}_\mathbf{x}(r)) = \\ &\quad 2\left(\frac{1}{\hat{\rho}^2(n(\mathbf{x}))|W|}\sum_{i\neq j} e_K(x_i, x_j) I(||x_i - x_j|| \leq r)\right. \\ &\quad \left. - \frac{1}{\hat{\rho}^2(n(\mathbf{x})+1)|W|}\int_W t^w(u, \mathbf{x}, r)\lambda_{\hat{\phi}}(u, \mathbf{x})du\right) \end{aligned} \tag{8}$$

where $\hat{\rho}^2(n(\mathbf{x})) = n(\mathbf{x})(n(\mathbf{x}) - 1)/|W|^2$, $n(\mathbf{x})$ number of points in W, $e_K(u, v)$ is the edge correction, $t^w(u, \mathbf{x}, r) = \sum_j e_K(u, x_j) I(||u_i - u_j|| \leq r)$ is a weighted count of the points of x that are r-close to the location u. In Baddeley et al. (2011), (8) is shown to become

$$\frac{n(\mathbf{x})^2}{2|W|}(\hat{K}_\mathbf{x}(r) - \pi r^2)$$

The compensator K-function is based on the fitted model and if it is correct the residual summary statistics should be on average zero. In terms of hypothesis testing using the residual K-function, the comparison is between the fitted model under the null hypothesis, and a hybrid of the current fitted model with a Strauss process under the

alternative hypothesis. In this case, a peak of the residual K-function at a particular distance r suggests that the current model may be improved including a Strauss process component, with interaction range r.

The residual G-function is the difference between the non-parametric estimate of the G-function and its compensator version based on the fitted model. It is equivalent to a score test where the null hypothesis is under the fitted model, and the alternative hypothesis is a hybrid of the current model with a Geyer process with saturation parameter $s = 1$.

Usually the residual K and G functions are represented graphically with upper and lower limits. The null distribution of the standardized residual is not known and the critical bands are approximate two-standard deviation limits under the fitted model, however the bands are unreliable for small values of r. It is possible to use simulations to obtain exact significance bands, but it is computationally demanding (Baddeley et al. 2013).

Summing up, the diagnostic plots based on the residual K and G functions should be used to decide which component has to be added at each step to the hybrid model. Indeed, these graphs show for which spatial distances the model has a lack of fit in describing the interaction between points.

In the **spatstat** package (Baddeley and Turner 2005) of R, we can find all the necessary functions that have been used for model fitting, prediction, simulation and model validation of hybrid models.

3 The study area and the geological information

Earthquakes are the most unpredictable damaging natural disaster. An earthquake is a sudden break and movement in the earth lithosphere due to the release of stress accumulated along tectonic plates, faults or volcanic areas. Earthquake damage is caused by the shaking of the ground generated by seismic waves that reach the earth surface. The level of damages mainly depends on the earthquake magnitude, the hypocentral depth, the epicentral distance and on the local shallow geology, which can generate local amplification.

Hellenic seismicity is generated by relative compressional motion between the African and Eurasian plates started at Oligo-Miocene time, about 26 Ma (million years) ago (Meulenkamp et al. 1988). The African plate is subducting beneath the Aegean lithosphere with a relative velocity of about 4 cm per year (Le Pichon and Angelier 1979) (see Fig. 1) forming the Hellenic Subduction Zone (HSZ) and the chain of volcanic island in the South Aegean Sea (Hellenic Volcanic Arc, HVA). The HSZ is the main source of earthquakes dominated by shallow

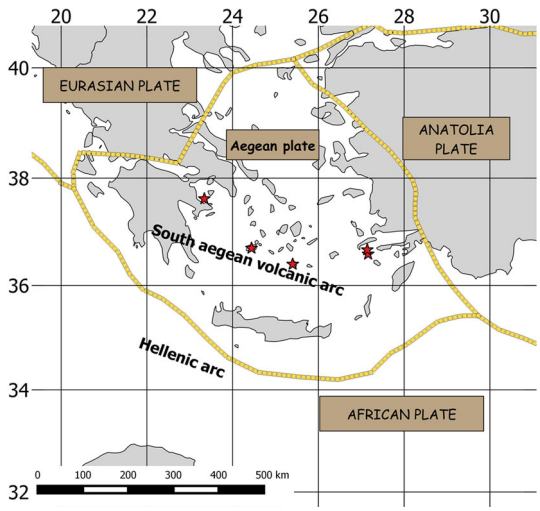

Fig. 1 Tectonic plates in the Hellenic region and *red stars* indicate the main volcanic centers

intraplate seismicity within the Aegean plate, interplate seismicity along the plate contact and by intermediate deep seismicity along the subducting African slab. Moving from West to East, the main volcanoes of the HVA are Methana, Milos, Santorini, Yali and Nisyros Siebert and Simkin (2014) (see Table 1). In general, the seismicity activity along the HVA is smaller in terms of magnitude than the seismic activity along the HSZ. Most of the volcanoes of the HVA are not active in terms of eruptions but are sources of microseismic activity (Bohnhoff et al. 2006; Dimitriadis et al. 2009).

In this study, the class of hybrid models proposed in Baddeley et al. (2013) are applied to the study of the Greek-Hellenic seismicity, an area of high seismic hazard characterized by both tectonic and volcanic seismogenic sources. The Hellenic arc is the most seismically active area of the European-Mediterranean region having experienced many destructive earthquakes. In the last century at least a dozen of earthquakes have affected the Greek area with devastating consequences (Papazachos et al. 1997). The most destructive earthquake occurred in 1926 (M_S 7.4) at about 115 km of depth just beneath the Hellenic volcanic Arc (Ambraseys and Adams 1998), in 1933 (M_W 6.6) with the epicentre near the Kos island (M_W 6.6 Papazachos et al. 1997) and in 1956 (M_S 7.4) located in the central Santorini-Amorgos graben. Recently, Greece was affected by an important seismic sequence characterized by two main earthquakes (both MW 6.0) occurred within eight days, on the 26th January and the 3rd of February, 2014 (Sokos et al. 2015).

Hellenic seismicity is monitored by four seismological centres: the Institute of Geodynamics and the Seismological Laboratories of the Universities of Athens, Thessaloniki

Table 1 The main volcanoes in the south Aegean volcanic arc moving from West to East

Name	Lat	Long	Elevation (m)	Type
Methana	37.62	23.34	760	Lava domes
Milos	36.70	24.44	751	Stratovolcano
Santorini	36.40	25.40	367	Shield volcano
Yali	36.67	27.14	180	Lava domes
Nisyros	36.59	27.16	698	Stratovolcano

and Patras. In the beginning of 2005, a national project was launched to unify the seismological networks in Greece (the Hellenic Unified Seismological Network, HUSN). The HUSN is nowadays constituted by about 150 seismic stations adequately distributed over the area to be monitored and by portable stations moved according to the investigation requirements (D'Alessandro et al. 2011).

Focal parameters of the earthquake occurring in the Hellenic region are routinely determined from the analysis of data recorded by the HUSN, and the earthquakes catalogue for the area contains events from 1964 up to nowadays. The accuracy and precision with which such parameters (hypocenter coordinates and event magnitude) are determined is mainly a function of the earthquake magnitude and of the number and distribution of the seismic stations. Small magnitude earthquakes are generally recorded from few stations (only the nearest ones) and consequently, focal parameters are not estimated reliably. Given the purpose of the work, in order to ensure a dataset as homogeneous as possible, in terms of data quality and reliability of focal parameters, in our analysis we have considered only earthquakes occurred in the Hellenic region between 2005 and 2014, with magnitude equal or greater than 4. So fixing this value of the magnitude, we study the spatial intensity of the main events occurred in the area excluding the micro and the minor events according to a qualitative classification of the magnitude.

Considering a period of 10 years, we also analyze and describe in a proper way the spatial interactions between points, neglecting time. We selected this time period not only for a technical reason due to the unification of the seismological networks, but also for having a good trade-off between a sufficient number of points and the model complexity that is related to the computational efficiency. Moreover aggregating over a longer time interval, the scale of aggregation observed in Fig. 2 changes and the clusters or gaps observed could be cancelled out giving a different interpretation of the phenomenon (Illian et al. 2008).

We additionally considered spatial geological information available in the area to understand dependence between events and the different sources of earthquakes.

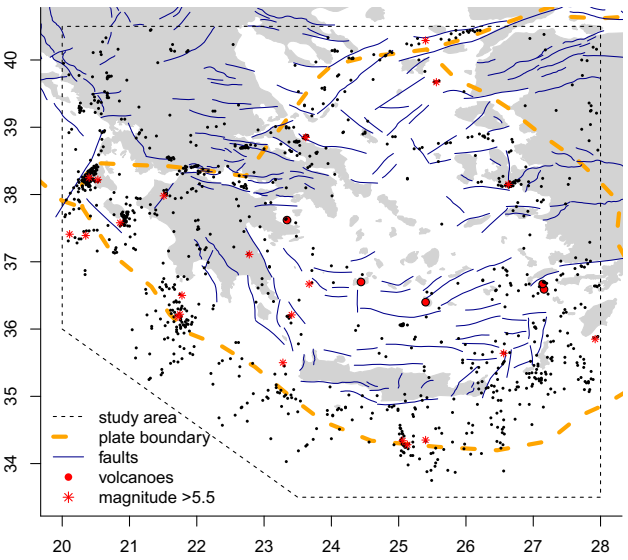

Fig. 2 Faults, plate boundary and main volcanoes in the Hellenic area. The *dotted black line* indicates the study window. The points are the observed events with a magnitude greater or equal than 4, *red stars* indicate points with a magnitude greater than 5.5

Table 2 List of the spatial covariates and p-values for the Berman test

Var	Description	p-value
D_{pb}	Distance to the plate boundary	0
D_f	Distance to the nearest fault	0
D_v	Distance to the nearest volcano	0.880

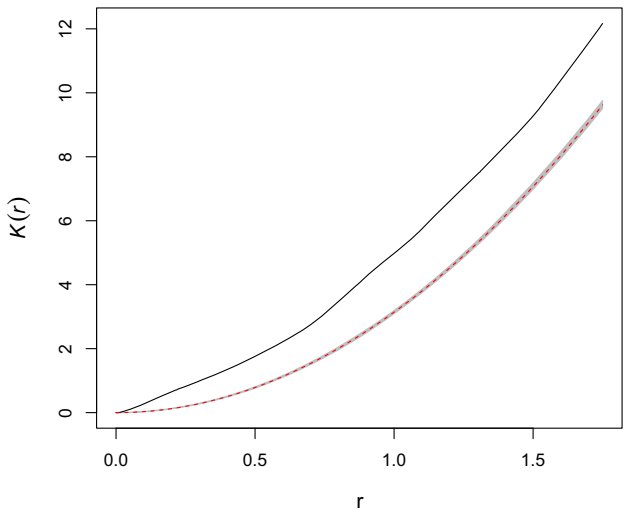

Fig. 3 The envelope of the K-function (*shaded region*) to test complete spatial randomness (CSR) condition of the earthquake events

In Fig. 2, the dotted line is the Aegean plate boundary coming from a digitalized global set of present plate boundaries on the earth (Bird 2003). Furthermore, we used

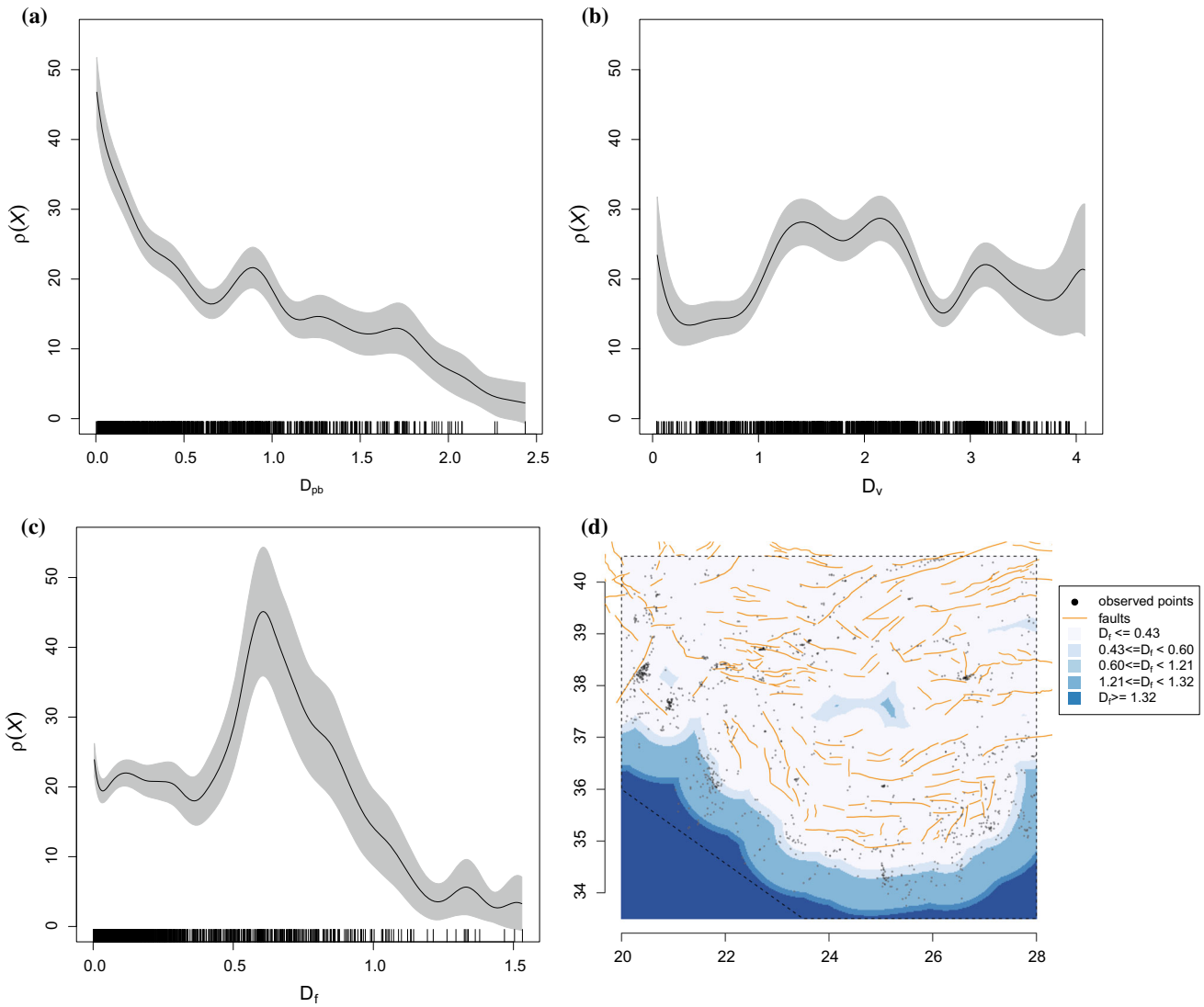

Fig. 4 Smoothed estimates of the intensity of the point process, as a function of the spatial covariates, distance to the plate boundary (**a**), the nearest volcano (**b**) and the nearest fault (**c**). Discretization of the spatial variable D_f (distance to the nearest fault) (**d**)

the Greek Database of Seismogenic Sources (GreDaSS) that concerns tectonic and active-fault data in Greece and its surroundings (Caputo et al. 2013). Generally, a 'fault' is a fracture in the earth along which the two blocks of crust have been moved relative to each other. The term 'active-faults' refers to faults in which a displacement has occurred in the recent geologic time ('seismogenic sources') or to areas assumed to be capable of producing moderate to strong earthquakes ('capable faults'). A capable fault will eventually become seismogenic sources in the future, and a seismogenic source was a capable fault, and usually the study of these is of interest in the seismic hazard analysis. An active fault has been identified integrating different available piece of information coming from historical and instrumental seismicity data, geological, structural, morphotectonic, paleoseismological and geophysical investigations.

The database provides metadata associated to each fault such as geometric (strike, dip, width, depth) and kinematic (rake) parameters and descriptive information (e.g. comments, latest earthquakes). In our analysis we considered the spatial shape file about the faults associated to the Composite Seismogenic Sources (CSS), see Fig. 2. We note that the seismogenic sources are not homogeneous in all the Hellenic area because the historical information is richer in the most populated areas and it is difficult to detect in offshore regions, e.g. the Aegean Sea.

Since in our analysis we want to detect whether and how the intensity depends on the geological information, we converted the spatial information on the faults, the plate boundary and the volcanoes into distance functions. For example using the information about coordinates of the volcanoes, we computed a spatial covariate that indicates

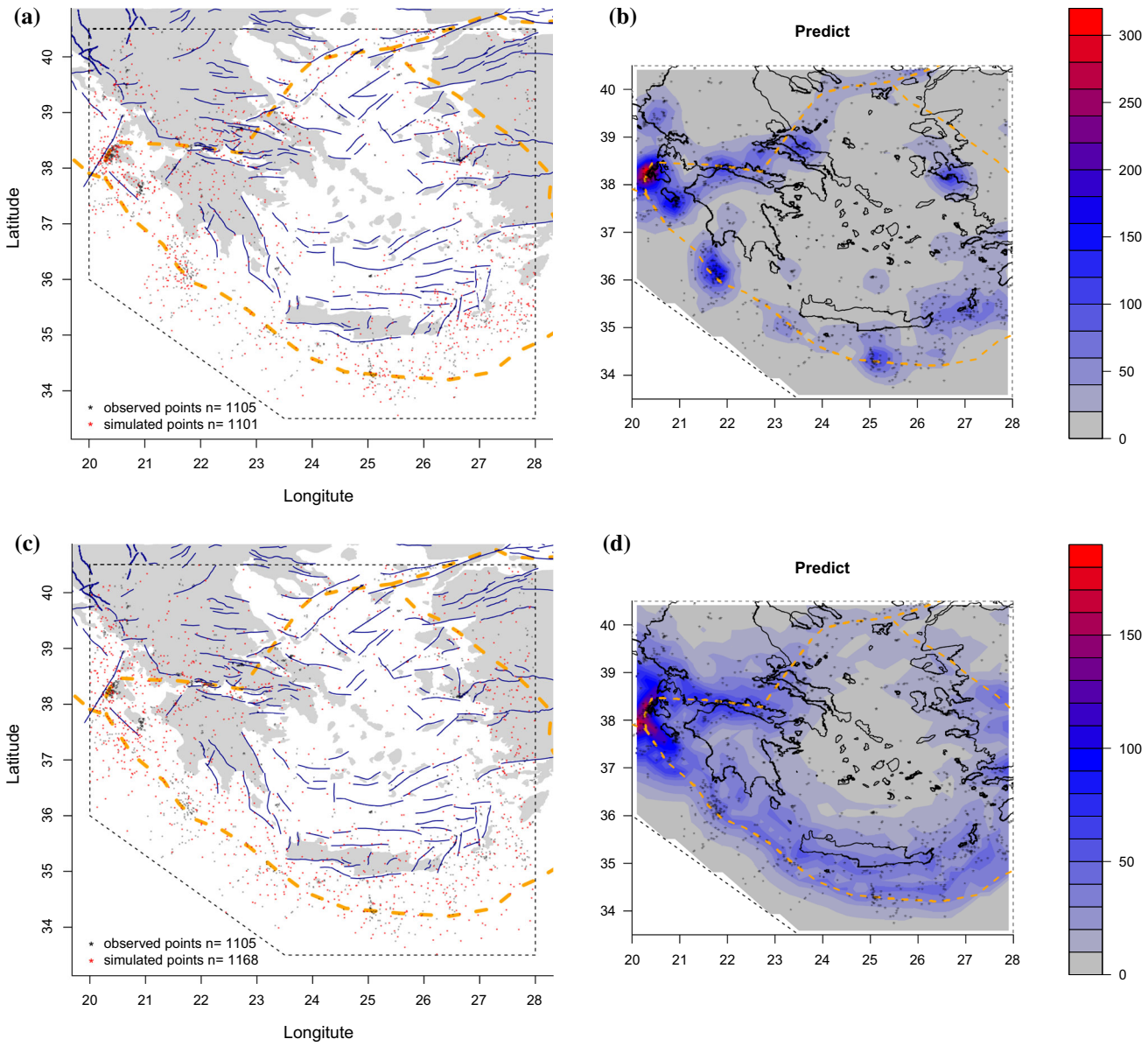

Fig. 5 Plot of observed and simulated events (**a**) and estimated spatial trend (**b**) for the model $ModPoisson_a$. Plot of observed and simulated events (**c**) and estimated spatial trend (**d**) for the model $ModPoisson_b$

for a generic location u in W the distance to the nearest volcano. In Table 2, the three spatial covariates are reported.

4 Results

4.1 Descriptive analysis

The events in the study window with a magnitude greater or equal than 4 between 2005 and 2014 define a spatial point pattern with 1105 events. Distances were computed considering geographical coordinates (longitude and latitude) and expressed in kilometres to interpret and comment the main results. The pattern has a clear spatial inhomogeneity and multi-scale interactions between points, for instance most of the events are around the plate boundary and we can visually identify clusters of events with a magnitude greater than 5.5 (Fig. 2).

Figure 3 shows the non-parametric empirical K-function and the corresponding envelope that was obtained considering the K-function for a large number of simulated patterns assuming complete spatial randomness and the same intensity of the observed pattern. The upper and lower envelopes are the pointwise maximum and minimum of the

simulated values of the K-function. It is clear that the observed pattern is not a Poisson process since the empirical K-function is outside the shadow region.

The Berman test (Berman 1986; Baddeley and Turner 2005) is used to assess the dependence of a point process on a spatial continuous covariate. Table 2 shows the corresponding p-values indicating that the variable D_v (distance to the nearest volcano) indicates that this variable is not significant to add valued information to the spatial intensity of the process. In Fig. 4b, the previous result is confirmed as the smoothed estimate of the intensity as a function of the distance to the nearest volcano is basically constant. Instead, the intensity of the point process decreases exponentially moving away from the plate boundary (variable D_{pb}). The intensity has a piecewise trend with respect to D_f (distance to the nearest fault) with a peak at degree distance of 0.6 (around 65 km) that corresponds to the events that lie in the south part of the study region around the plate boundary. Considering a segmented linear regression between D_f and the intensity, we found the following breakpoints in terms of degree distances $\phi = \{0.43, 0.60, 1.21, 1.32\}$ for which there is a change in the sign of the slope (Muggeo 2003, 2008). Figure 4d shows the discretization of the spatial covariate D_f, where the points in the study region for which $(\phi_i \leq D_f < \phi_{i+1})$ have a distance to the nearest fault between ϕ_i and ϕ_{i+1}.

4.2 Statistical inference and modeling proposal

4.2.1 Inhomogeneous Poisson models

The first attempt in model estimation is to fit an inhomogeneous Poisson model with intensity depending on the spatial covariates, that is equal to equation (6) where the term $G(\cdot)$ is null.

Table 3 $ModPoisson_a$-estimated parameters for the inhomogeneous Poisson point process model with Gaussian kernel estimator for x and y and bandwidth values $(h_x, h_y) = (0.22, 0.19)$

	Estimate		Zval
(Intercept)	0.2433	***	3.57
D_{pb}	−0.1153		−1.78
$I(D_f < \phi_1)D_f$	−1.2557	***	−3.72
$I(\phi_1 \leq D_f < \phi_2)D_f$	−0.0633		−0.28
$I(\phi_2 \leq D_f < \phi_3)D_f$	−0.4000	**	−3.21
$I(\phi_3 \leq D_f < \phi_4)D_f$	−0.8222		−1.78
$I(D_f \geq \phi_4)D_f$	−0.3021		−1.28
AIC	−6382.877		
No. of simulated points	1101		
Range of raw residuals	[−1.91; 2.33]		

Note: * p < 0.1; * p < 0.05; *** p < 0.01

According to the descriptive results, we considered the spatial covariates assuming that the log of the intensity depends linearly on D_{pb} and piecewise linearly on D_f.

As for the general trend with respect to the coordinates (x and y), we considered both a parametric polynomial trend and a non-parametric trend, this last computed using a Gaussian kernel estimator selecting the bandwidth values with the methods indicated in Sect. 2.2 (cross-validated bandwidth selection, likelihood cross-validation, Scott's rule and FLP method). Comparing different semi-parametric models in terms of AIC, the model with kernel estimated using the FLP method performed better than the others and the obtained bandwidth values were $(h_x, h_y) = (0.22, 0.19)$. On the other hand, for the full parametric model, a second-order polynomial in x and y for the spatial trend fits reasonably good (see Table 4 and Fig. 5c, d). We note that using a higher-order polynomial drives into computational errors in the estimation of the Fisher information matrix.

We selected the significant covariates comparing nested models in terms of the residual deviance. The estimated parameters θ_1 for the inhomogeneous Poisson process both with a kernel estimation ($ModPoisson_a$) and a second-order polynomial ($ModPoisson_b$) with respect to x and y are reported in Tables 3 and 4, respectively. Using the spatial kernel, the significant variables are D_{pb} and some of the component of the piecewise linear regression in D_f, whilst using a polynomial trend all the spatial covariates are significant. The estimated parameters of the models are not

Table 4 $ModPoisson_b$-estimated parameters for the inhomogeneous Poisson point process model with a second-order polynomial with respect to the coordinates x and y

	Estimate		Zval
(Intercept)	−146.4664	**	−3.01
D_{pb}	−1.0124	***	−13.69
$I(D_f < \phi_1)D_f$	−2.8391	***	−8.15
$I(\phi_1 \leq D_f < \phi_2)D_f$	−1.3013	***	−5.10
$I(\phi_2 \leq D_f < \phi_3)D_f$	−1.6692	***	−10.52
$I(\phi_3 \leq D_f < \phi_4)D_f$	−2.4947	***	−5.28
$I(D_f \geq \phi_4)D_f$	−2.0786	***	−8.25
D_v	0.1887	*	2.01
x	0.3864		0.42
y	8.0901	***	3.90
x^2	0.0384	***	3.37
xy	−0.0611	***	−5.08
y^2	−0.0920	***	−3.63
AIC	−5247.943		
No. of simulated points	1168		
Range of raw residuals	[−5.77; 6.14]		

Note: * p < 0.1; ** p < 0.05; *** p < 0.01

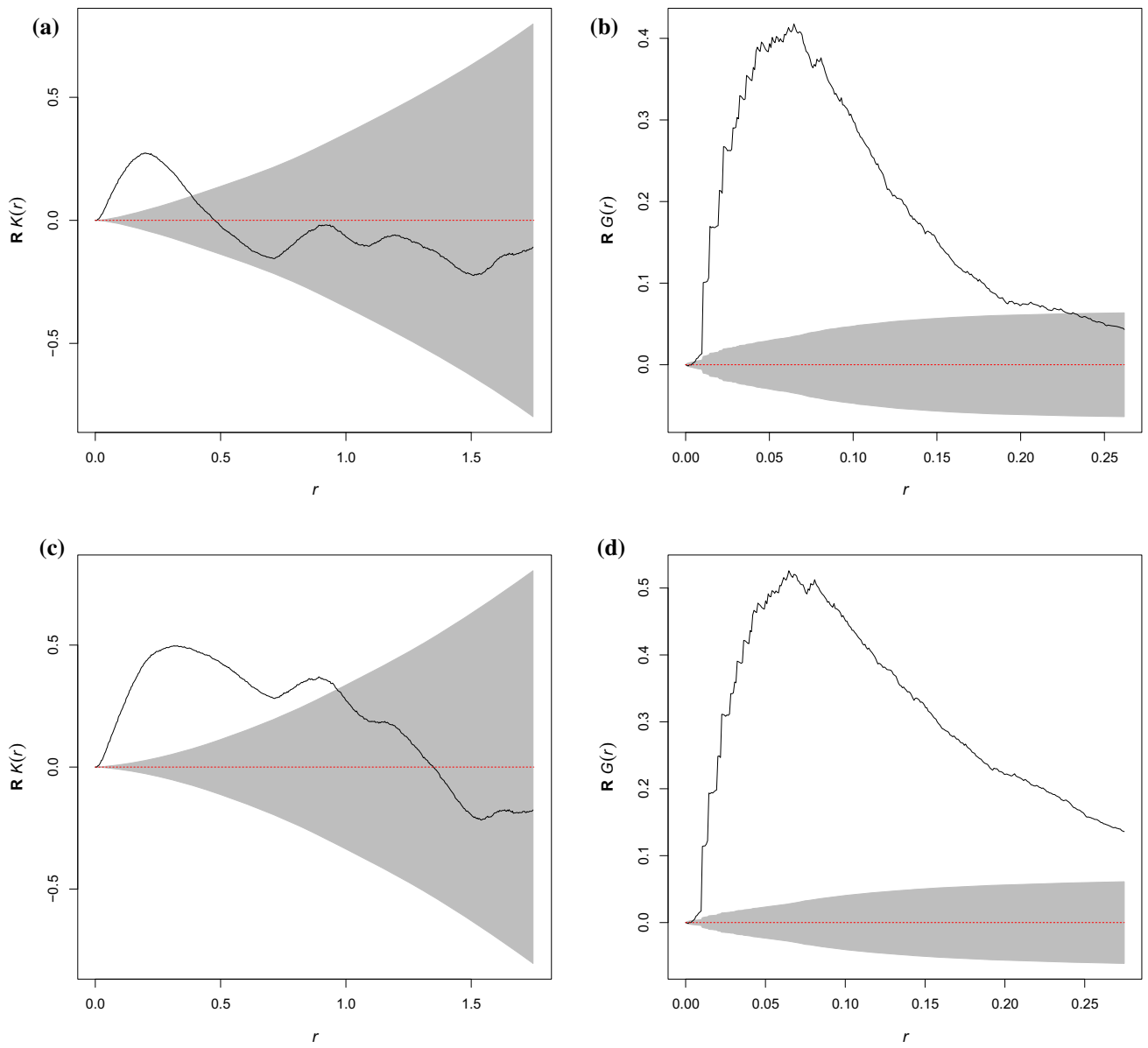

Fig. 6 The residual K and G functions for the inhomogeneous Poisson process models, with kernel-based spatial trend $ModPoisson_a$ (**a**, **b**), and second-order polynomial $ModPoisson_b$ (**c**, **d**) in the coordinates

Table 5 Estimated irregular parameters for the selected hybrid models: $ModHybrid_a$ and $ModHybrid_b$

Gibbs component	Irregular paramters			
	$ModHybrid_a$		$ModHybrid_b$	
	r_j	s_j	r_j	s_j
G_1 (Geyer)	0.04 (4.45 km)	11	0.05 (5.56 km)	15.5
G_2 (Geyer)	0.05 (5.56 km)	4.5	0.06 (6.67 km)	1.5
G_3 (Geyer)	0.06 (6.67 km)	2.5	0.09 (10.00 km)	11.5
G_4 (Geyer)	0.08 (8.90 km)	1.5	0.15 (16.68 km)	3.5
S (Strauss)	0.66 (73.39 km)			

directly comparable since they have two different spatial trends, however, in both cases, we can assert that increasing the distance to the nearest fault and to the plate boundary the intensity decreases. For both models, the number of simulated points is close to the observed one, but their spatial displacement does not capture the observed clusters (Fig. 5a, c) even with $ModPoisson_a$ that identifies the hotspots (Fig. 5d). For both models, the residual K and G functions show a specific trend that is far from zero for short distances. Indeed, these diagnostic tools show that the use of the inhomogeneous Poisson point process model is inappropriate since there is an unexplained interaction between points (Fig. 6), that reflects a positive association between the events. Reminding that the residual K and G functions are related to score test for model comparisons, the current Poisson models may be improved adding some components accounting for interaction, such as a Strauss component or a Geyer one. Therefore it could be interesting to consider more complex models, like hybrids, that account for the interaction between points, also at multiple scales, more properly.

4.2.2 Inhomogeneous hybrid models

We then considered hybrid models introduced in Sect. 2.1 in order to better explain the observed interpoint interaction. The challenge here is to choose a combination of Gibbs process components that explains well the spatial observed pattern. Hybrid models are fitted incrementally adding one component density at a time. The form of the residual K or G functions helps in identifying the appropriate Gibbs component. For both models ($ModPoisson_a$ and $ModPoisson_b$), the residual G function has a specific trend that is far from zero for short distances with higher values for r between 0.05 and 0.1 (around 5.6 and 10.1 km). We thus tried several combinations of Geyer (4) and Strauss (3) processes selecting the irregular parameters (η) by maximum profile pseudolikelihood. We searched the interaction radius in the range $0.01 \leq r \leq 2$, and for the Geyer process the saturation parameter varied from 1 to 20, $s = 1, 1.5, \ldots, 19.5, 20$. To consider the inhomogeneity degree, we estimated two models taking into account the spatial covariates, one with a non-parametric kernel-based trend in the coordinates ($ModHybrid_a$) and the other one with a quadratic polynomial trend with respect to the coordinates of the points ($ModHybrid_b$). A number of nested models were compared in terms of the residual deviance. Table 5 shows the irregular parameters (η) for the best selected models, and Tables 6 and 7 show the corresponding estimated regular parameters θ.

$ModHybrid_a$ represents a hybrid process based on multitype Geyer processes (four components) and a Strauss process which describes adequately the multi-scale interactions between the events. For this model the estimated irregular parameters (η) are nine as shown in Table 5. Moreover the parametric vector θ in (6) has six elements, the intercept term (θ_1) and five interaction parameters (θ_2), one for each process in the hybrid model. For the Geyer processes, the interaction parameters are greater than 1, confirming a multi-scale clustering dependence between points for interaction distances less or equal than 8.9 km. For a larger interaction radius, the events show a CSR behavior since the γ parameter associated to the Strauss

Table 6 $ModHybrid_a$-estimated parameters for the Hybrid model with a kernel term for the spatial trend in x and y

	Estimate	γ_j		Zval
(Intercept)	−0.2858		***	−3.62
G_1	0.0835	1.09	***	8.24
G_2	0.1523	1.16	***	4.27
G_3	0.1835	1.20	**	2.92
G_4	0.3004	1.35	***	4.13
S	−0.0112	0.97	***	−9.25
AIC	−7371.777			
No. of simulated points	1191			
Range of raw residuals	[−1.63; 2.03]			

Note: * p < 0.1; ** p < 0.05; *** p < 0.01

Table 7 $ModHybrid_b$-estimated parameters for the Hybrid model with a second-order polynomial trend in x and y

	Estimate	γ_j		Zval
(Intercept)	8.7863			0.45
G_1	0.0841	1.09	***	12.06
G_2	0.4627	1.59	***	8.06
G_3	0.1193	1.13	***	12.22
G_4	0.1968	1.22	***	6.51
D_{pb}	−0.2656		***	−6.25
$I(D_f < \phi_1)D_f$	−1.0196		***	−4.15
$I(\phi_1 \leq D_f < \phi_2)D_f$	−0.4963		*	−2.38
$I(\phi_2 \leq D_f < \phi_3)D_f$	−0.5362		***	−4.39
$I(\phi_3 \leq D_f < \phi_4)D_f$	−1.1964		*	−2.54
$I(D_f \geq \phi_4)D_f$	−1.0059		***	−4.97
x	−1.1664		*	−2.42
y	0.5004			0.63
x^2	0.0273		***	5.48
xy	−0.0045			−0.55
y^2	−0.0065			−0.75
AIC	−7121.841			
No. of simulated points	1475			
Range of raw residuals	[−1.62; 2.29]			

Note: * p < 0.1; ** p < 0.05; *** p < 0.01

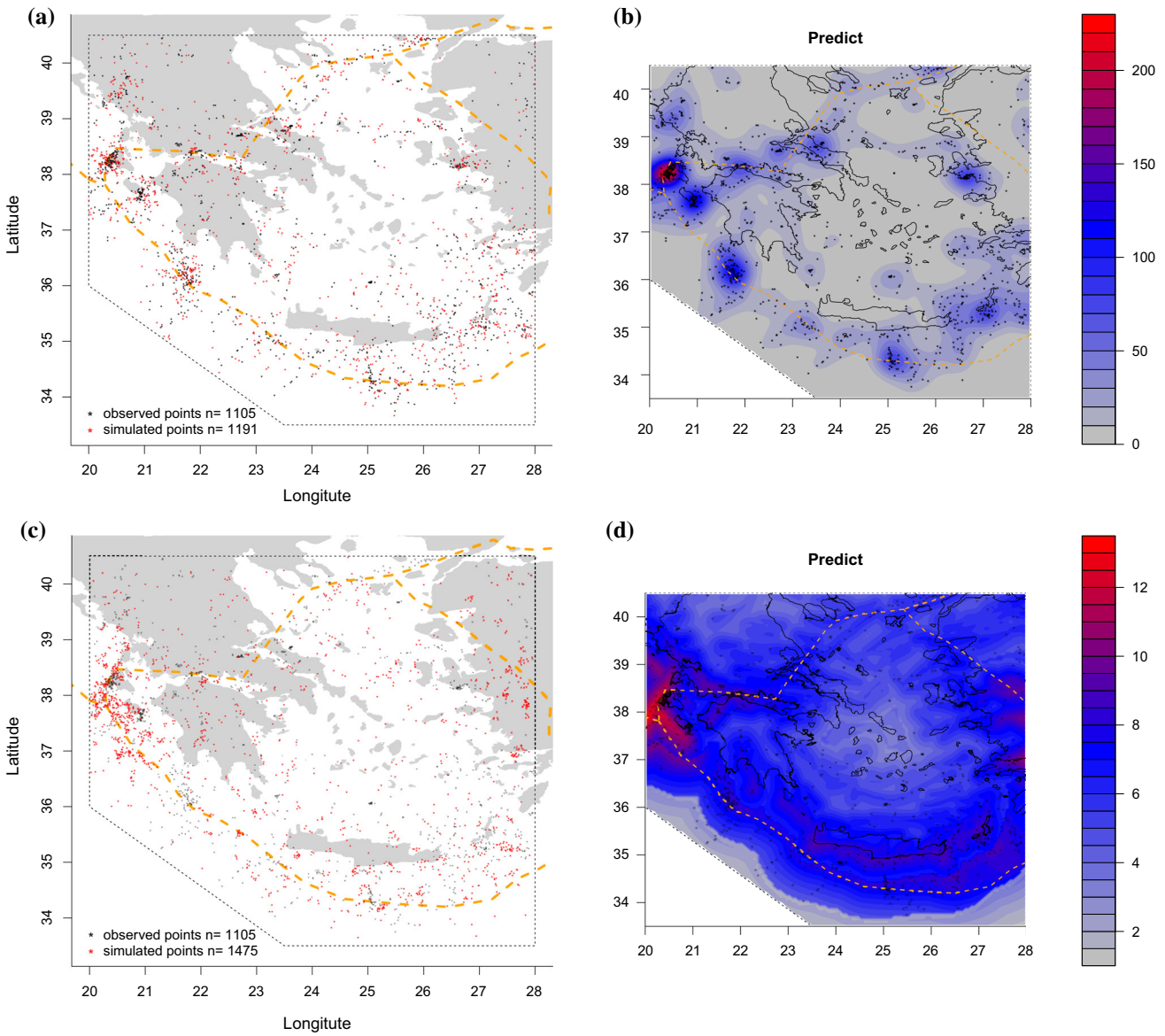

Fig. 7 Plot of observed and simulated points (**a**) and estimated spatial trend (**b**) for the model $ModHybrid_a$. Plot of observed and simulated points (**c**) and estimated spatial trend (**d**) for the model $ModHybrid_b$

process is not significatively different from 1. Using a hybrid model with a non-parametric kernel-based term in x and y and smoothing parameters estimated by FLP, the covariates are not significant.

On the other hand, $ModHybrid_b$ represents a model based on a hybrid of four Geyer components that have an interaction parameter greater than 1. For this model, the total number of estimated irregular parameters (η) are eight and the parametric vector (θ) has eleven parameters to explain the trend part and four interaction effects one for each Geyer process. In this case, the variables D_f and D_{pb} are significant and both of them are negatively related to the log spatial intensity.

More in detail, increasing the distance from the plate boundary to 50 km $(r = 0.4496)$, the spatial conditional intensity decreases by 1.13. In an area around the faults less than 50 km, the log intensity decreases by 0.046 increasing the distance to the nearest fault by 5 km. The trend for the intensity is decreasing for an area that has points with a distance greater than 50 km to the faults; indeed, all the parameters for the piecewise linear trend with respect to D_f are negative and significant. Close to the faults, we have a

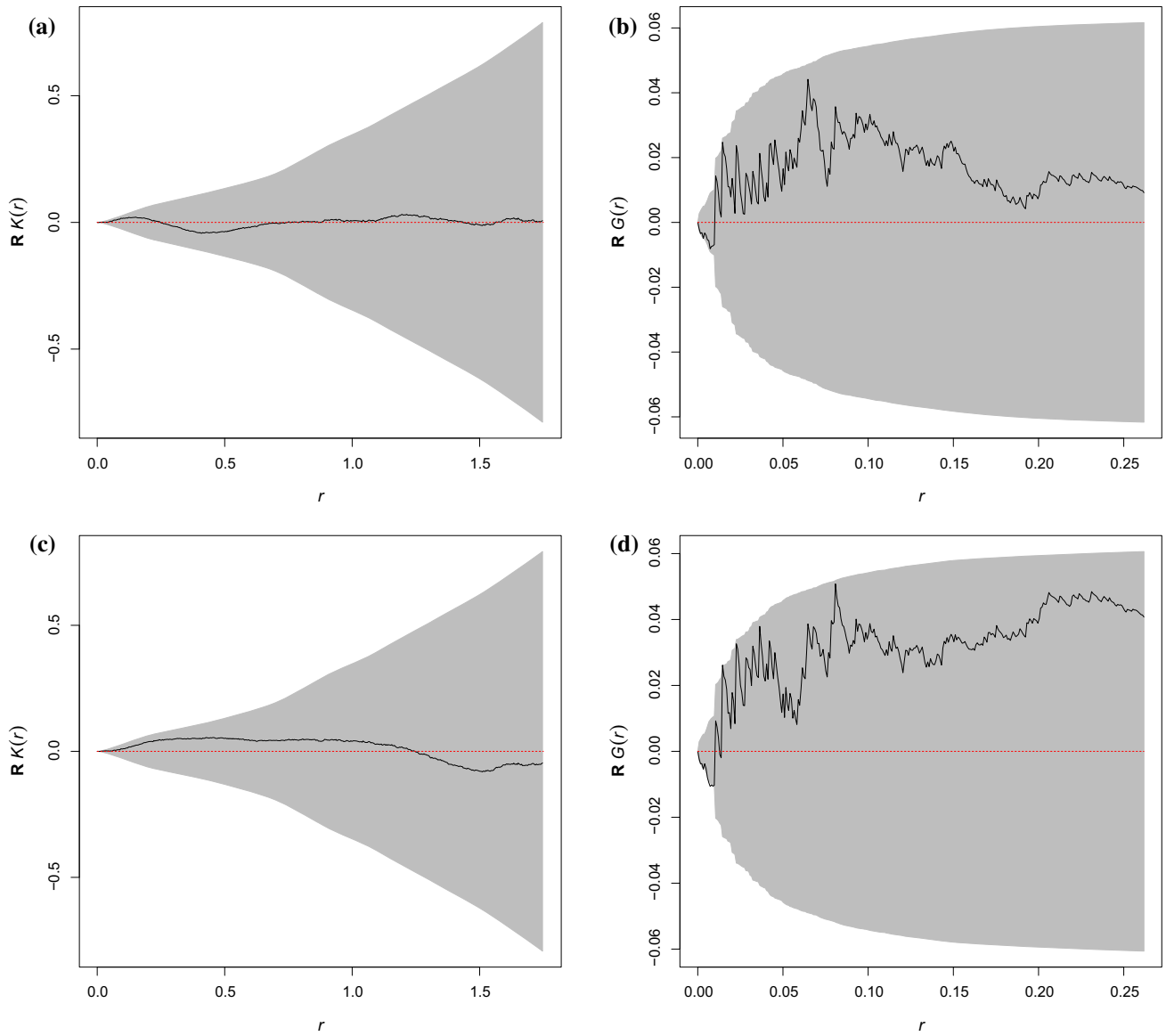

Fig. 8 The residual K and G functions for the hybrid models with kernel-based spatial trend $ModHybrid_a$ (**a**, **b**), and second-order polynomial $ModHybrid_b$ (**c**, **d**) in the coordinates

more rapid reduction of the intensity than in the neighborhood of the plate boundary.

In both the hybrid models, we can observe that the number of simulated points is greater than the number of observed ones, especially for $ModHybrid_b$. However the higher number of simulated points affects marginally the residual K and G functions and their upper and lower limits. We notice that under the parametric formulation assuming both a Poisson and a hybrid process, the number of simulated points are greater than 1105. It is due to the fact that considering covariates information in the model all the different seismogenetic source of earthquakes can generate points, even if in reality only some of them had generated earthquakes.

Considering both hybrid models, we have an improvement in terms of *AIC* with respect to both models based on the inhomogeneous Poisson process. Indeed the AIC decreases by 988 for model $ModHybrid_a$ and by 1874 for model $ModHybrid_b$. Moreover we observe a sensible reduction of the range of the spatial raw residuals for the model $ModHybrid_b$ even though the number of simulated points is slightly larger than the number of events in the observed pattern Fig. 7.

Now the residual K and G functions, shown in Fig. 8, oscillate around zero and they are inside the envelopes indicating that the interaction structure between the earthquakes is well described by both models.

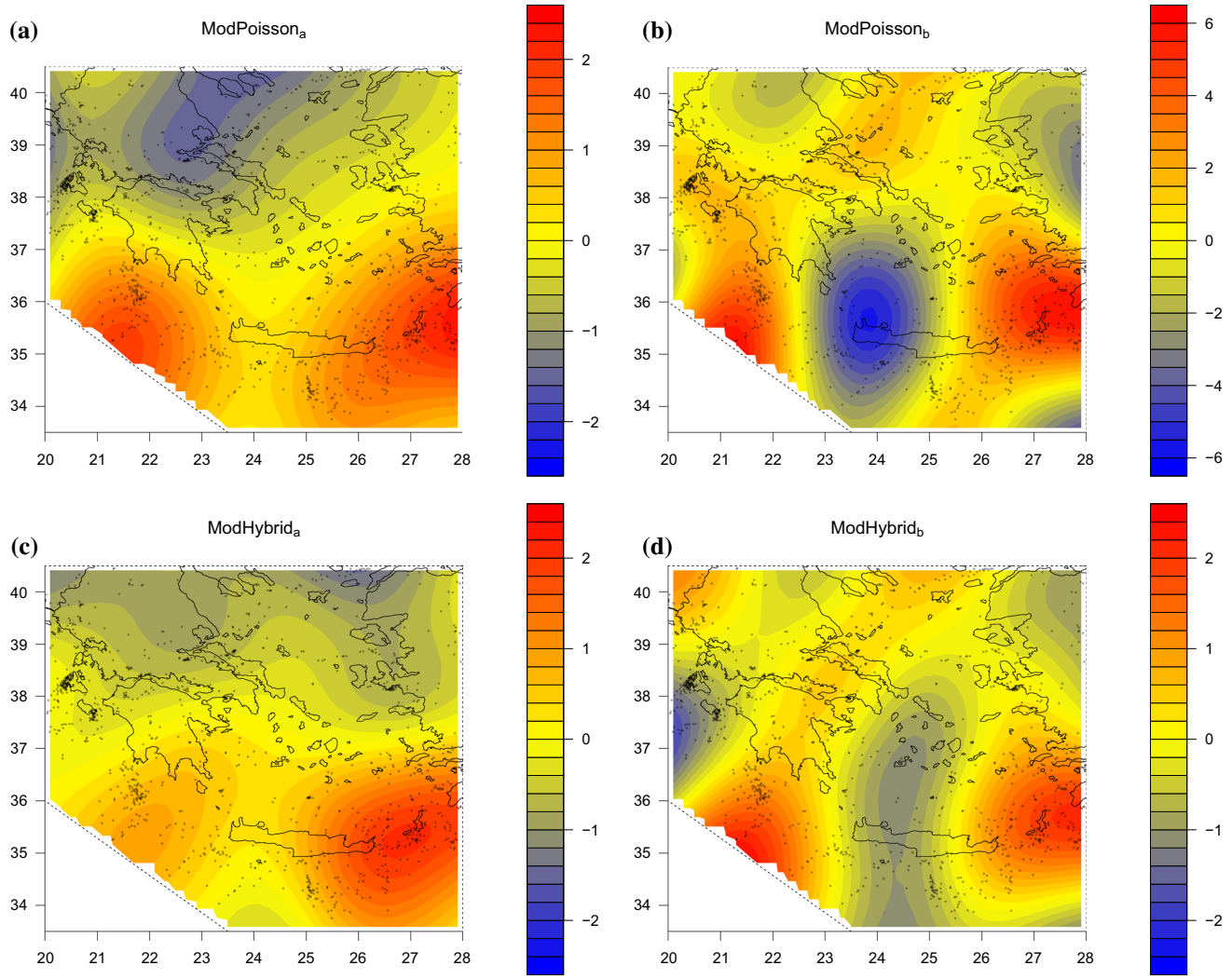

Fig. 9 Plot of smoothed raw residuals for $ModPoisson_a$ (**a**), $ModPoisson_b$ (**b**), $ModHybrid_a$ (**c**) and $ModHybrid_b$ (**d**)

5 Conclusions and final remarks

The novelty of this work is the application of hybrids of Gibbs point process models to describe the spatial distribution of earthquake events (with a magnitude ≥ 4) in the Hellenic area from 2005 to 2014. Since the spatial distribution of the events is relatively complex and it seems that the different sources of earthquakes (faults, active tectonic plate and volcanoes) produce events with different spatial displacements and orientations, we characterize the multi-scale interaction between the earthquakes and the relationship between the conditional spatial intensity and the geological information available in the study area. The spatial variables used in the analysis are: distance to the nearest fault, the distance to the nearest volcano and the distance to the plate boundary. After considering simple inhomogeneous Poisson models (too simple to provide a good fit), we found two suitable inhomogeneous hybrid models that are good in terms of AIC, of range of raw residuals, and of residual K and G functions. The first hybrid model ($ModHybrid_a$) has a kernel smoothed trend in x and y with bandwidth values estimated with the *FLP* (Forward likelihood prediction) method. On the other hand, we also fitted a hybrid parametric model with a second-order spatial polynomial trend and spatial covariates ($ModHybrid_b$). We found that the variable that indicates the distance to the nearest volcano is not significant in explaining the spatial intensity, in fact the volcanic Hellenic arc area is mostly characterized by microseismic activity. Increasing the distance to the plate boundary and to the fault, the conditional intensity decreases, and this reduction is greater if we are close to faults. As for the interaction aspect between points, both models agree in identifying a multi-scale clustering between points for interpoint distances approximately less than 10 km.

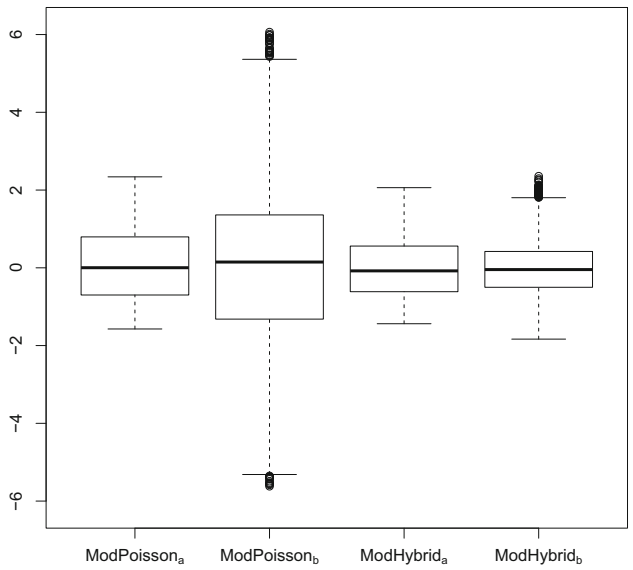

Fig. 10 Boxplots of smoothed raw residuals for $ModPoisson_a$, $ModPoisson_b$, $ModHybrid_a$ and $ModHybrid_b$

The estimated spatial trends for the two models are significantly different because the first model reproduces exactly the observed trend and hotspots, while the second model gives a smoother information for all the study area.

To further compare the models, we computed image plots and boxplots of the raw residuals, that are shown in Figs. 9 and 10, respectively. According to these results, moving from Poisson to hybrid models we have improvements in terms of range, variability and reduction of specific spatial trend in the raw residuals. Comparing the two final models, $ModHybrid_a$ seems slightly better than $ModHybrid_b$ since it has a higher AIC. Moreover the spatial raw residuals of $ModHybrid_a$ have a smoother spatial trend (Fig. 9c) compared to what happens in Fig. 9d, in fact $ModHybrid_b$ has a few number of residuals with high values.

Summing up, if the research interest focuses on the description of the spatial intensity of the phenomena and therefore on the study of the interaction between earthquake events, the model based on a non-parametric spatial trend estimated by FLP seems more suitable. On the other hand, if the main interest is to study and to understand how the several seismogenic sources of earthquakes influence the spatial intensity of the phenomena a full parametric model would be more appropriate.

As for future work, some possible extensions could regard an improvement of the structure of the full parametric model considering in a proper way the interaction between covariates. In fact the distance to the nearest fault and the distance to the plate boundary for the observed points are not independent and they present an exponential relationship. Moreover, it would be of interest trying to subdivide the study region into macro areas characterizing the structure of interaction between points in these different areas because we expect that the multi-scale cluster between events is different for points that occur along the plate boundary than points that occur in the neighbourhood of faults. Another possible extension could be to consider a spatio-temporal formulation of hybrid models and also including depth information. However performing a spatial partition, and assuming a multi-type hybrid Gibbs process, as well as considering an extension in space and time, needs a more detailed methodological formulation.

Acknowledgments This research was partially developed during the traineeship at the Istituto Nazionale di Geofisica e Vulcanologia funded by "PROGRAMMA OPERATIVO CONVERGENZA 2007-2013 FONDO SOCIALE EUROPEO (MISURA 3)" and this work was partially funded by Grant MTM2013-43917-P from the Spanish Ministry of Science and Education. We thank the reviewers for providing constructive comments and helping in improving the quality of this paper.

References

Adelfio G (2010) An analysis of earthquakes clustering based on a second-order diagnostic approach. In: Palumbo F et al (eds) Data analysis and classification. Springer, Berlin, pp 309–317

Adelfio G, Chiodi M (2009) Second-order diagnostics for space-time point processes with application to seismic events. Environmetrics 20(8):895–911

Adelfio G, Chiodi M (2015a) Alternated estimation in semi-parametric space-time branching-type point processes with application to seismic catalogs. Stoch Environ Res Risk Assess 29(2):443–450

Adelfio G, Chiodi M (2015b) Flp estimation of semi-parametric models for space-time point processes and diagnostic tools. Spat Stat 14:119–132

Adelfio G, Schoenberg FP (2009) Point process diagnostics based on weighted second-order statistics and their asymptotic properties. Ann Inst Stat Math 61(4):929–948

Ambraseys N, Adams R (1998) The rhodes earthquake of 26 June 1926. J Seismol 2(3):267–292

Anwar S, Stein A, van Genderen J (2012) Implementation of the marked strauss point process model to the epicenters of earthquake aftershocks. Advances in geo-spatial information science Taylor & Francis, London, pp 125–140

Baddeley A, Møller J (1989) Nearest-neighbour markov point processes and random sets. Int Stat Rev 57(2):89–121

Baddeley A, Turner R (2005) Spatstat: an r package for analyzing spatial point patterns. J Stat Sofw 12(6):1–42

Baddeley A, Turner TR (2000) Pratical maximum pseudo likelihood for spatial point patterns (with discussion). Aust N Z J Stat 42(3):283–322

Baddeley A, Turner R, Møller J, Hazelton M (2005) Residual analysis for spatial point processes. J R Stat Soc Ser B 67(5):617–666

Baddeley A, Gregori P, Mateu J, Stoica R, Stoyan D (2006) Case studies in spatial point pattern modelling. Lecture Notes in Statistics, Springer, New York, p 185

Baddeley A, Rubak E, Møller J (2011) Score, pseudo-score and residual diagnostics for spatial point process models. Stat Sci 26(4):613–646

Baddeley A, Turner R, Mateu J, Bevan A (2013) Hybrids of gibbs point process models and their implementation. J Stat Softw 55(11):1–43

Baddeley A, Rubak E, Turner R (2015) Spatial point patterns: methodology and applications with R. Chapman and Hall, London

Badreldin N, Uria-Diez J, Mateu J, Youssef A, Stal C, El-Bana M, Magdy A, Goossens R (2015) A spatial pattern analysis of the halophytic species distribution in an arid coastal environment. Environ Monit Assess 187(5):1–15

Berman M (1986) Testing for spatial association between a point process and another stochastic process. Appl Stat 35(1):54–62

Besag J (1975) Statistical analysis of non-lattice data. Statistician 24(3):179–195

Besag J (1977) Some methods of statistical analysis for spatial data. Bull Int Stat Inst 47(2):77–92

Bird P (2003) An updated digital model of plate boundaries. Geochem Geophys Geosyst 4:1027

Bohnhoff M, Rische M, Meier T, Becker D, Stavrakakis G, Harjes HP (2006) Microseismic activity in the hellenic volcanic arc, greece, with emphasis on the seismotectonic setting of the santorini-amorgos zone. Tectonophysics 423(1):17–33

Caputo R, Chatzipetros A, Pavlides S, Sboras S (2013) The greek database of seismogenic sources (gredass): state-of-the-art for northern greece. Ann Geophys 55(5):859–894

Chiodi M, Adelfio G (2011) Forward likelihood-based predictive approach for space-time processes. Environmetrics 22:749–757

Chiodi M, Adelfio G (2014) etasflp: Estimation of an etas model. mixed flp (forward likelihood predictive) and ml estimation of non-parametric and parametric components of the etas model for earthquake description. R package version 1.0.2

Cox DR, Isham V (1980) Point processes. Chapman and Hall, London

D'Alessandro A, Papanastassiou D, Baskoutas I (2011) Hellenic unified seismological network: an evaluation of its performance through snes method. Geophys J Int 185(3):1417–1430

Daley DJ, Vere-Jones D (2007) An introduction to the theory of point processes: general theory and structure. Springer Science & Business Media, New York

Dimitriadis I, Karagianni E, Panagiotopoulos D, Papazachos C, Hatzidimitriou P, Bohnhoff M, Rische M, Meier T (2009) Seismicity and active tectonics at coloumbo reef (aegean sea, greece): monitoring an active volcano at santorini volcanic center using a temporary seismic network. Tectonophysics 465(1):136–149

Geyer CJ (1999) Likelihood inference for spatial point processes. Stoch Geom 80:79–140

Hawkes A, Adamopoulos L (1973) Cluster models for erthquakes-regional comparison. Bull Int Stat Inst 45(3):454–461

Illian J, Penttinen A, Stoyan H, Stoyan D (2008) Statistical analysis and modelling of spatial point patterns. Wiley, New York

Jensen JL, Moller J et al (1991) Pseudolikelihood for exponential family models of spatial point processes. Ann Appl Probab 1(3):445–461

Le Pichon X, Angelier J (1979) The hellenic arc and trench system:a key to the neotectonic evolution of the eastern mediterranean area. Tectonophysics 60(1):1–42

Meulenkamp J, Wortel M, Van Wamel W, Spakman W, Strating EH (1988) On the hellenic subduction zone and the geodynamic evolution of crete since the late middle miocene. Tectonophysics 146(1):203–215

Møller J, Waagepetersen R (2004) Statistical inference and simulation for spatial point processes. Chapman & Hall/CRC, London

Muggeo VM (2003) Estimating regression models with unknown break-points. Stat Med 22(19):3055–3071

Muggeo VM (2008) Segmented: an R package to fit regression models with broken-line relationships. R News 8(1):20–25

Ogata Y (1988) Statistical models for earthquake occurrences and residual analysis for point processes. J Am Stat Assoc 83(401):9–27

Papazachos V, Papazachos B, Papazachou C, Papazachou K (1997) The earthquakes of Greece. Ziti, Thessaloniki

R Development Core Team (2005) R: A language and environment for statistical computing. R Foundation for Statistical Computing, Vienna. http://www.R-project.org, ISBN 3-900051-07-0

Ripley BD (1976) The second-order analysis of stationary point processes. J Appl Probab 13(2):255–266

Ripley BD (1988) Statistical inference for spatial processes. Cambridge University Press, Cambridge

Ripley BD, Kelly FP (1977) Markov point processes. J Lond Math Soc 15:188–192

Siebert L, Simkin T (2014) Volcanoes of the world: an illustrated catalog of holocene volcanoes and their eruptions. Smithsonian Institution, Global Volcanism Program Digital Information Series, GVP-3. http://volcano.si.edu/search_volcano.cfm

Silverman BW (1986) Density estimation for statistics and data analysis. Chapman and Hall, London

Sokos E, Kiratzi A, Gallovič F, Zahradník J, Serpetsidaki A, Plicka V, Janskỳ J, Kostelecký J, Tselentis GA (2015) Rupture process of the 2014 cephalonia, greece, earthquake doublet (mw6) as inferred from regional and local seismic data. Tectonophysics 656:131–141

Strauss DJ (1975) A model for clustering. Biometrika 62(2):467–475

Vere-Jones D (1978) Earthquake prediction: a statistician's view. J Phys Earth 26:129–146

Ye X, Yu J, Wu L, Li S, Li J (2015) Open source point process modeling of earthquake. In: Bian F, Xie Y (eds) Geo-informatics in resource management and sustainable ecosystem. Springer, Berlin, pp 548–557